Insertion Tasks using an Aerial Manipulator

Christopher Korpela, Matko Orsag, Todd Danko, and Paul Oh

***Abstract*— This paper demonstrates insertion tasks using an aerial vehicle affixed with a multi-degree of freedom manipulator. Using a combined strategy of visual servoing and force feedback compliance, the aerial manipulator achieves peg-in-hole insertion while attached to a validation test rig. A strongly coupled control scheme between the aircraft and manipulator is mandated for tasks requiring millimeter accuracy. Visual servoing is well-established for both ground and aerial vehicles and facilitates the large aircraft-arm motions. Force feedback upon contact with the environment provides compliant insertion and smaller motions in the presence of position error. We present recent results demonstrating and validating peg-in-hole insertion using the proposed aircraft-arm model and system.**

I. Introduction

Insertion tasks represent a classic control experiment that are well-known, have been widely studied by the ground robotics community, and can be easily benchmarked for comparison. Some common applications include inserting a power plug into a socket, changing a light bulb, or placing a bolt into a structure. Ground-based mobile manipulators have solved these problems with sub-millimeter accuracy [1]. The ground-based system must coordinate the vehicle and arm motions to perform these tasks. While the coupling between the environment (i.e. insertion point) and robot does influence the vehicle base with added contact forces/torques and friction, the base can typically maintain stability during the entire motion.

However, the loose coupling required during insertion greatly influences the dynamics of an aerial manipulator. Rigidity in the manipulator and the propagation of contact forces when interacting with the environment can cause crashes. There have been recent results where multi-DOF aerial manipulators have experienced coupling with the environment [2], [3]. Other groups have investigated compliance in assembly tasks [4], [5], [6] or dynamic stability and control [7], [8].

A combined strategy of visual servoing and force feedback is used to control the aircraft-arm system. An *eye-in-hand* camera servos the arm and aircraft towards the target using fiducials. Upon contact with the insertion point, force feedback provides insertion success back to the controller. A dithering method and peg-tilting enables the manipulator to "feel" for the insertion point. Peg-tilting is a common methodology where the cylinder is first titled to facilitate the initial insertion, aligning with respect to the holes and then finally pushed through [9].

Manuscript received March 10, 2014. This project was supported in part by a US NSF CRI II-New, Award # CNS-1205490, DoD Advanced Civil Schooling, and a U.S. Fullbright Scholarship.

C. Korpela, T. Danko, and P. Oh are with the Drexel Autonomous Systems Lab, Drexel Univeristy, Philadelphia, PA 19104 USA {cmk325, twd25}@drexel.edu, paul@coe.drexel.edu

M. Orsag is with Faculty of Electrical Engineering and Computing, University of Zagreb, 10000 Zagreb, Croatia morsag@fer.hr

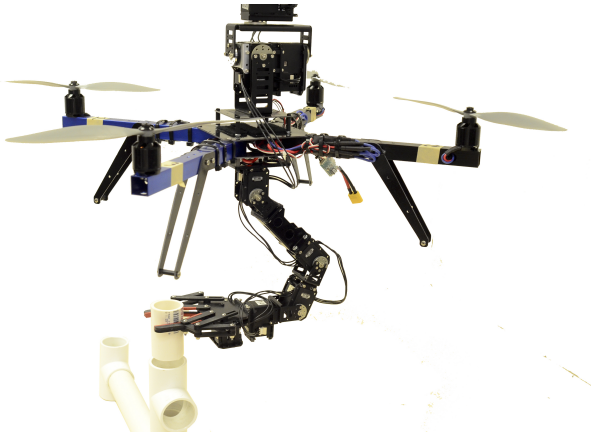

Fig. 1. MM-UAV in hover affixed to a 6-DOF overhead gantry

This paper presents a solution to the peg-in-hole problem from an aerial vehicle using a 3-DOF manipulator, dubbed MM-UAV (Mobile Manipulating Unmanned Aerial Vehicle). A control scheme to coordinate the coupled manipulator-aircraft system (Fig. 1) is validated to allow for the insertion of a peg into a hole. Section II details the kinematic and dynamic model for the aircraft and manipulator. Section III describes the proposed control architecture for the coupled system. The hardware and software components are found in Sec. IV. Section V presents system model testing and validation. Results are shown in Sec. VI.

II. Modeling

The rigid body dynamics of rotorcraft are well understood [10], [11]. Much of the previous work in quadrotor control assumes the geometric center and quadrotor center of mass are coincident. With the introduction of a manipulator, the center of mass shifts and the inertia properties change based on arm joint angles, added load masses, and environmental contact forces and torques.

A. Aircraft-Arm Kinematics

A generalized 6-DOF vehicle model is proposed. The world inertial frame W is fixed and the body reference frame B is placed at the vehicle center of mass as shown in Fig. 2. The position and orientation of the body frame with respect to the inertial reference frame can be expressed in standard form as $p_b = [x\ y\ z]^T$ and $\phi_b = [\psi\ \theta\ \varphi]^T$ where the frames are right-handed with Z pointed upward. Attitude is

978-1-4799-4605-1/14/$31.00 ©2014 IEEE

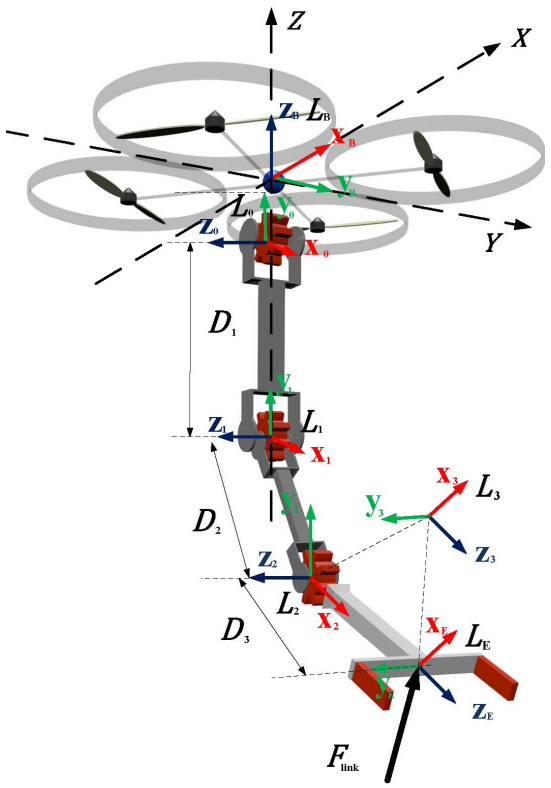

Fig. 2. Coordinate System (links expanded for clarity)

denoted by the yaw-pitch-roll Euler angles in the body frame $(Z\,Y\,X)$. The inertial frame is rotated by $R_b \in SO(3)$ to provide the orientation of the body frame.

$$R_b(\phi_b) = \begin{bmatrix} c_\psi c_\theta & c_\psi s_\theta s_\varphi - s_\psi c_\varphi & c_\psi s_\theta c_\varphi + s_\psi s_\varphi \\ s_\psi c_\theta & s_\psi s_\theta s_\varphi + c_\psi c_\varphi & s_\psi s_\theta c_\varphi - c_\psi s_\varphi \\ -s_\theta & c_\theta s_\varphi & c_\theta c_\varphi \end{bmatrix} \quad (1)$$

The manipulator is attached directly below the center of gravity of the quadrotor frame. Forward kinematics are derived using Denavit-Hartenberg (DH) parameters as shown in Table I. Parameters θ, d, a, and α are in standard DH convention and q_i for $i = 1$ to n are joint variables for the arm. The direct kinematics function relating the quadrotor body to the end-effector frame, p_e, is:

$$p_e = p_b + R_b p^b_{eb} \quad (2)$$

where p^b_{eb} is the position of the end-effector with respect to the body frame.

B. Aircraft-Arm Dynamics

The equations of motion for the center of mass of the geometric center of the generalized 6-DOF vehicle have the standard Newton-Euler form [12]:

$$\vec{F} = m_Q \dot{\vec{v}} + \mathbf{\Omega} \times m_Q \vec{v} \quad (3a)$$

$$\vec{\tau} = \mathbf{I}\dot{\mathbf{\Omega}} + \Omega \times \mathbf{I}\mathbf{\Omega} \quad (3b)$$

TABLE I

DENAVIT-HARTENBERG PARAMETERS FOR MANIPULATOR, WITH VIRTUAL JOINT L_3 THAT KEEPS A CONSTANT ROTATION $q_E = 0$, AND QUADROTOR BASE FRAME L_B

Link Number	θ (rad.)	d (mm)	a (mm)	α (rad.)
0	0	0	d_z	$\pi/2$
1	q_1	0	D_1	0
2	q_2	0	D_2	$\pi/2$
3	q_3	0	0	0
E	$q_E = 0$	D_3	0	0

where F represents the combination of propeller, aerodynamic, and gravitational forces with vehicle mass, m_Q, linear velocity, v, linear acceleration, $\dot{v}$, and rotational velocity, Ω. Torque, τ, is calculated from the inertia matrix, I, and the rotational velocity and acceleration, Ω and $\dot{\Omega}$ respectively. The torque and force produced from the quadrotor propellers have to be taken into account. The torque $\vec{\tau}^i$ has two components, one coming from the actual propeller drag Q, and the other due to the displacement of the propeller from the center of mass $\Delta\vec{\mathbf{o}}^i_{CM}(q_j)$. In an aerial manipulator system, the center of mass shifts as each joint (q_j) of the manipulator rotates and the torque becomes a nonlinear function of the manipulator joint angles:

$$\vec{\boldsymbol{F}}_q(u) = \sum_{i=1}^{4} \vec{\mathbf{F}}(u)^i \quad (4a)$$

$$\vec{\boldsymbol{\tau}}_q(u, q_j) = \sum_{i=1}^{4} \vec{\mathbf{Q}}(u)^i + \Delta\vec{\mathbf{o}}^i_{CM}(q_j) \times \vec{\mathbf{F}}(u)^i \quad (4b)$$

Given the dynamic model for both manipulator and the quadrotor body, a simplified arm model is utilized for the complete system. Quadrotor dynamics considered in this paper do not account for various aerodynamic effects (i.e. blade flapping, ground effect, etc.) experienced during highly dynamic flying maneuvers. Most of the vehicle's critical motions occur around hover outside of ground effect where the pitch and roll angles are effectively zero. This fact justifies a simplified mathematical model.

III. CONTROLLERS

A. Attitude Control

Taking into account the dynamics of the system, a simplified Proportional controller for the corresponding attitude loop, and a Proportional-Integral controller for the position loop is proposed. Effectively, this transforms the proposed two stage cascade controller structure into a single PI-Derivative position controller. The proposed PI-D controller equation (5) implies that the control difference $\vec{e}$ is taken through the proportional and integration channels, while the derivative channel is connected directly to speed measurements of the quadrotor $\vec{v}_0$. Equations are written in vector form because they are applied to x, y, z positions in 3D space.

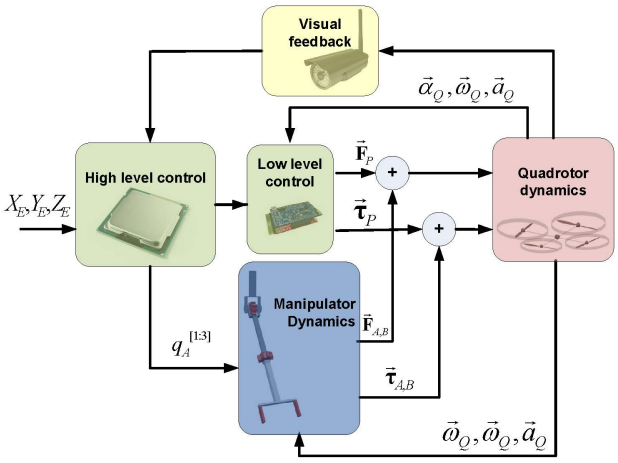

Fig. 3. MM-UAV Control Structure

$$\vec{u} = K_P\vec{e} + K_I \int \vec{e} + K_D\vec{v}_0 \tag{5}$$

K_P, K_I, and K_D are the PI-D control gains. Error vector $\vec{e}$ is the difference between the x, y, z position data and the actual setpoint reference values, and $\vec{v}$ is the speed measurement. Due to the fact that the derivation channel (i.e. aircraft speed) is error sensitive, leading the control difference directly through can cause serious problems and possibly damage the aircraft. On the other hand, position data is much more reliable and can be used directly in the control loop. PI-D position control is implemented as a Python class, running at a 20 Hz refresh rate.

B. Visual Servoing and Position Control

Image Based Visual Servoing (IBVS) has been extensively used by rotorcraft to achieve hover for surveillance and localization [13], [14]. An *eye-in-hand* system is used where the camera is attached to the end-effector. The camera frame relative to the end-effector frame is known *a priori* as shown in Fig. 4. The transformation between the image feature velocities, $\dot{s}$, and the joint velocities, $\dot{q}$, must be determined where:

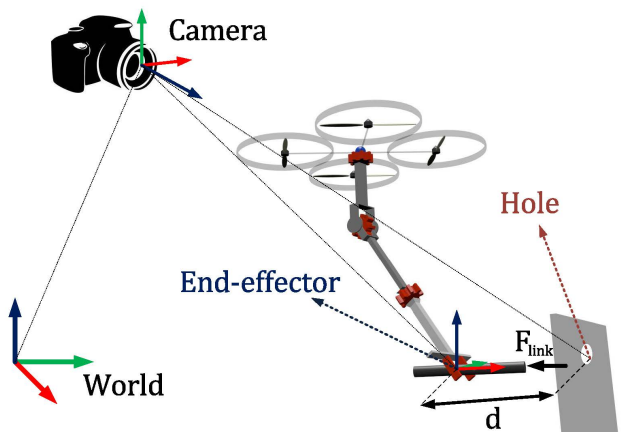

Fig. 4. Camera Reference Frame (camera in an exploded view for clarity)

$$s = J(x, y, Z, q)\dot{q} \tag{6}$$

The center location of the camera frame $(u,\ v)$ is projected into Cartesian coordinates where $C = (X_C,\ Y_C,\ Z_C)$ of the center of the hole. Using the center location, d is calculated to determine the distance of the target hole to the camera.

The control inputs consist of $x,\ y,\ z$ position and yaw ψ orientation of the quadrotor, yaw joint q_1, pitch joint q_2, and roll joint q_3 of the end-effector. The total controllable degrees of freedom for the aircraft-arm system is seven. As the wrist is spherical with intersecting axes of rotation, the inverse kinematic calculations are greatly simplified to determine joint angles for a desired pose and orientation. The arm can be described as a series of transforms:

$$T = A_{0T} = A_{01}A_{12}(q_1)A_{23}(q_2)A_{3T}(q_3) \tag{7}$$

where A_{01} is the fixed transform from the center of a quadrotor and A_{3T} is the transform from the last joint of the arm (q_3) to the tool tip. A_{AB} is the transform from joint A to joint B and is driven by the angle of joint $A(q_A)$. With the vehicle at a specified position and yaw orientation, the next step is to solve for the spherical wrist joints (q_1, q_2, q_3) using the method described in [15]. The first step in this process is to identify the transform that represents the combined joint rotations from the wrist to the target (A_{3T}) where:

$$A_{3T} = A_{3T}^{-1} \tag{8}$$

Next, q_1, q_2, and q_3 are calculated directly from A_{3T} where:

$$q_1 = atan2(A_{3T}[2,3], A_{3T}[1,3]) \tag{9a}$$

$$q_2 = atan2(\sqrt{(A_{3T}[1,3]^2 + A_{3T}[2,3]^2}, A_{3T}[3,3]) \tag{9b}$$

$$q_3 = atan2(A_{3T}[3,2], -A_{3T}[3,1]) \tag{9c}$$

to generate the closed form solution for the joint angles.

C. Force Feedback

An impedance control strategy is proposed to control the dynamic interaction between the manipulator and its environment. Impedance control enables contact between the manipulator and its environment while maintaining stability during the transition from free motion to interaction [16]. In a simplified manner, the manipulator can be seen as mass-spring-damper system behaving like an impedance towards the environment. The controller applies prescribed interaction forces at the end effector which are calculated as:

$$F_{int} = K[X_0 - X] \tag{10}$$

where F_{int} is the desired interaction force to be applied at the end effector, and $X_0 - X$ is the position error and K is a stiffness gain to map between position error and interaction force. K can be thought of as a spring constant while $X_0 - X$

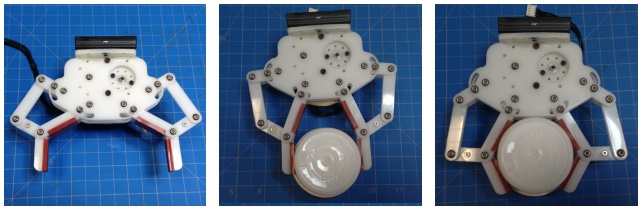

(a) Jaws Open (b) Pinching Grasp (c) Passively Compliant Caging Grasp

Fig. 5. Passively compliant 2 degree of freedom gripper with 1 degree of actuation

can be thought of as the spring's compression. (10) can be rearranged to solve for a pseudo-goal position to command the end effector to, using the position controller that will impart the desired amount of force. To achieve this, we need to calculate the torques necessary to command each joint where:

$$T_{act} = J^{\#T} F_{int} \tag{11}$$

Combining 10 and 11, we have:

$$T_{act} = J^{\#T} K[X_0 - X] \tag{12}$$

to represent overall commanded joint torques.

IV. Hardware and Software Design

The aircraft-arm system is constructed using a quadrotor (3DRobotics), a single 3-DOF manipulator, and a web camera. The vehicle contains the Arduino-based APM 2.6 autopilot with 880Kv brushless motors and 11 inch propellers. Power and communications are tethered providing for a greater payload capacity and fast messaging to the control station. The autopilot maintains a local control loop while the higher level processing is done off-board. An ultrasonic range finder provides altitude measurements. Final construction is shown in Fig. 1.

The manipulator is assembled using off-the-shelf Dynamixel servo motors, girders, and brackets. The hand is a custom designed gripper with two degrees of freedom and 1 degree of control. A single Dynamixel servo motor controls the opening and closing of the fingers, while a spring mechanism allows the fingers to passively conform around convex objects. This is accomplished by allowing the finger tips to close inward after the knuckle joints have collided with the grasped object. A mechanical stop prevents the fingers from opening wider than a parallel jaw configuration making the hand suitable for performing pinch grasps as shown in Fig. 5.

Software is integrated through a ROS infrastructure. Using the provided node based and message exchange system, it is easy to build the control system and establish communication between the aircraft and ground station. The mavlink protocol operates at 115k baud while the control loop runs at 20 Hz. Dynamixels use the controller package provided by ROS and the web camera leverages OpenCV libraries.

V. System Validation

To test and validate the control architecture, the system was first implemented on a gantry system as shown in Fig. 6. Dubbed MM-SISTR (Mobile Manipulating-SISTR), the gantry is modeled after the Systems Integrated Sensor Test Rig (SISTR) [17], [18]. SISTR was developed as a hardware-in-the-loop test rig and designed to be used to evaluate obstacle detection sensors (LIDAR, computer vision, ultrasonic, ultra-wideband radar, millimeter wave radar, etc.), design sensor suites, and test collision avoidance algorithms.

The gantry can traverse 0.35 m/s along each x, y, and z axis. To provide yaw, pitch, and roll angles and velocities for the emulated aircraft, a 3-DOF gimbal is attached to the gantry z-axis. MM-SISTR can be tuned for almost any rotorcraft model in hover or near-hover modes. Models to account for ground-effect can also be incorporated to study perturbations and disturbances. For this particular analysis, a quadrotor model was chosen due to their simplicity in mechanical operation and the symmetry of their construction. The actual vehicle is 50 cm in diameter and weighs 1.5 kg.

Using a recursive Newton-Euler algorithm and neglecting friction forces, one can derive generalized force/torque equations produced from each joint movement of the manipulator:

$$\sum_{j=0}^{n}[D_{ij}(\mathbf{q})\ddot{q}_j]+\sum_{k=0}^{n}\sum_{j=0}^{n}[C^i_{kj}(\mathbf{q})\dot{q}_k\dot{q}_j]+h_i(\mathbf{q}) = \tau_i, 0 \leq i \leq n \tag{13}$$

with D_{ij} as a generalized inertia tensor, C^i_{kj} is the generalized Coriolis and Centrifugal force matrix and h_i is a generalized gravity force.

Given that τ_0 calculates forces produced on the aircraft body (i.e. $w = \tau_0$), Newton-Euler analysis provides the necessary tools to calculate static and dynamic disturbances acting on the rotorcraft. In a complete model, Newton-Euler equations for manipulator motion need to be provided with initial angular and linear speeds and accelerations. To simplify the overall problem, we make a reasonable assumption that the aircraft is in hover during manipulation.

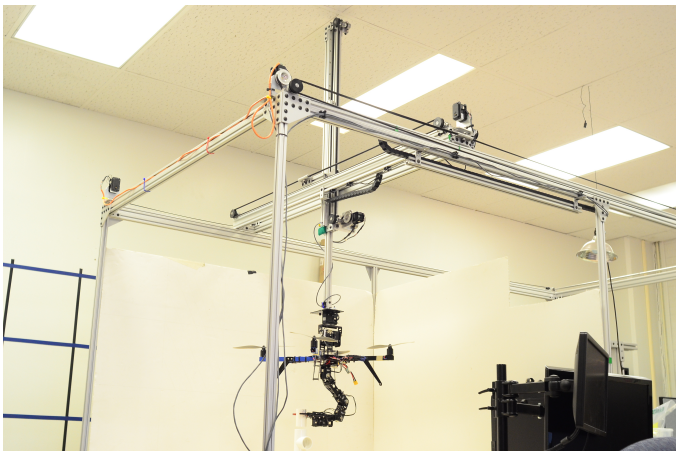

Fig. 6. MM-SISTR test and evaluation gantry rig

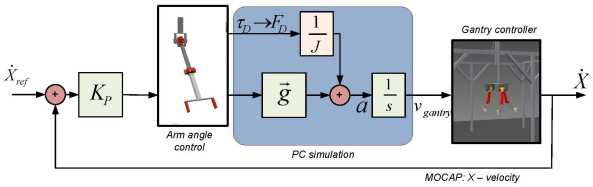

Fig. 7. Angle Attitude Controller

This assumption enables us to regard the initial linear and angular dynamics of the aircraft body as zero, thus effectively decoupling the dynamics.

A. Applied Torque Model

The 6-DOF gantry utilizes a torque model to reproduce the reactions the aircraft undergoes when subjected to moments applied by the manipulator, interactions with the environment, or added load masses. The 3-axis torso provides yaw-pitch-roll position, velocity, torque, and impedance feedback and control. The applied torque is tuned according to the mass and inertial properties of the vehicle. A rotorcraft with a larger mass and inertia will be able to withstand larger pitch and roll moments compared to a vehicle with less mass and inertia. The basic assumption for the quadrotor in hover is that the thrust force and the force of gravity are equal:

$$\sum_{i=1}^{4} \vec{F_i} = m_Q \cdot \vec{g}, \tag{14}$$

where $\vec{g}$ represents the gravity acceleration vector. The quadrotor translates by tilting slightly in the desired direction. Therefore, for a small angle approximation, x and y coordinate dynamics can be derived. For clarity, we are showing only x axis dynamics (i.e. force in the x direction F_x and respective acceleration a_x), produced from the quadrotor pitch angle Θ.

$$\begin{aligned} F_x = m \cdot g \sin(\Theta) \sim m_Q g \Theta \\ a_x \sim g\Theta \end{aligned} \tag{15}$$

Because the aircraft interacts with the environment, the applied torques are fed into the simulated aircraft model. The attitude controller ultimately needs to compensate and correct these disturbances. Both static (constant torque applied by the manipulator mass) and dynamic (moving torques associated with articulation and environmental contact) are sensed by the attitude controller. This approach allows us to write a simple dynamic model for the emulation of quadrotor dynamics seen in Fig. 7.

The disturbance force, F_D is mapped from the applied torque, τ_D, which contributes to the linear acceleration, a_x, of the vehicle base. J is the inertial tensor for the 6-DOF aircraft. The linearized equation for $\tau_D \mapsto F_D$ mapping can be derived from the complete dynamic model of the arm in (13). The acceleration resulting from the torque distance has the form:

$$a_x = g\Theta + \frac{\tau_D \mapsto F_D}{J} \tag{16}$$

Moments applied to the aircraft first introduce changes to angular positions and velocities which change the thrust vector. This altered thrust vector then causes a lateral translation in the vehicle. The torso joint positions adjust accordingly to emulate the pitching and rolling motions and the gantry provides the linear displacement in the x and y directions. Direct forces such as aerodynamic effects, propeller wash or ground effect, and wind gusts are not modeled. The forces and torques that do influence the vehicle pose are environmental contact through the end-effector, added load masses, and the mass and inertia of the manipulator itself.

B. Velocity Control Loop

The reference velocity is set by the user through a joystick interface. This velocity is compared to the actual gantry velocity provided by a motion capture system. The error is fed into a PID controller which calculates the angular position required to translate the gantry and eliminate the error. The angle is projected onto the linear axis as acceleration through the gravity vector. The angular position of the aircraft changes in the same direction as the applied force. The measured torque, converted into a disturbance force and divided by the system mass, also contributes to the linear acceleration. An integrator converts acceleration into velocity which is sent to a gantry controller to actuate the gantry motors. Since the inertia properties are used to calculate the emulated UAV velocity, the controller can be tuned for almost any rotorcraft.

VI. Experimental Results

A. Peg Insertion

A series of peg-in-hole experiments were performed for model verification. The peg is a plastic PVC cylinder with an outer diameter of 1.6 in that fits into a PVC t-joint. The peg fits snug into the fixed cylinder. Fig. 8 shows a series of snapshots during a vertical insertion tasks. Cartesian coordinates were sent to the controller specifying the insertion point. When the peg makes contact with the cylinder, compliance in the wrist joints allow for insertion.

B. Controller Performance

Fig. 9 shows the applied torques to the UAV body, elbow joint, and wrist joint of the arm. When the arm makes contact with the cylinder, the contact force is propagated through the arm back to the vehicle. The arm pitch joints (elbow and wrist) experience torque spikes between time stamps 40 and 60 during contact with the PVC pipe. Just after time stamp 60, the peg is inserted and the applied torque is quickly reduced. At time stamp 90, the peg is removed showing greater torques applied again to the pitch joints.

VII. Conclusions

In this paper an arm-aircraft system is presented and validated using peg-in-hole insertion tasks. One of the primary goals of this research is to capture and compensate for reactionary forces applied to a rotorcraft during interactions with the environment. The system kinematics and dynamics

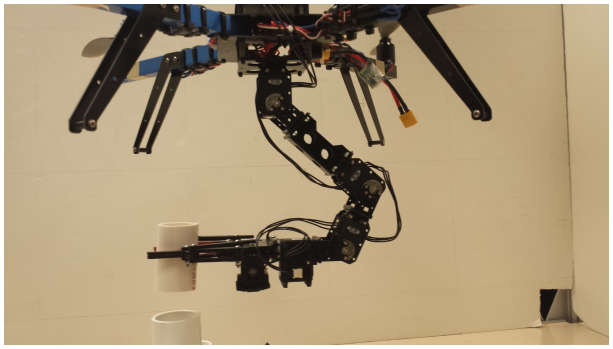

(a) Approach

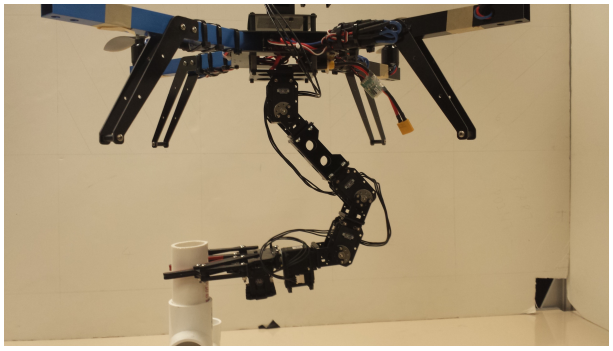

(b) Initial contact

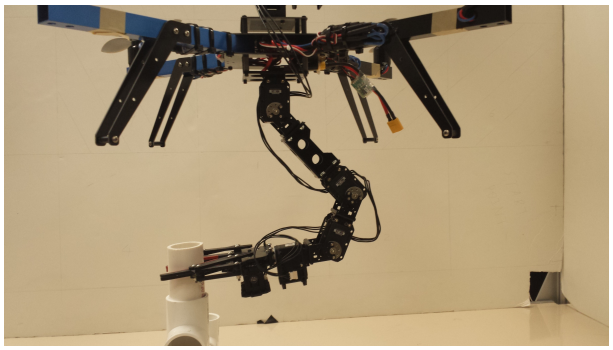

(c) Insertion

Fig. 8. Vertical insertion task

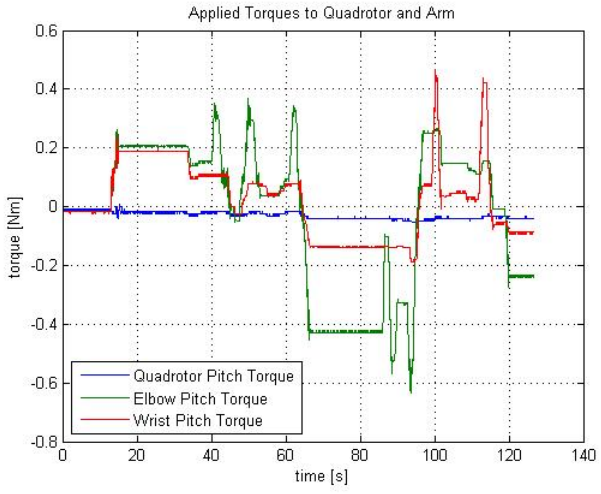

Fig. 9. Quadrotor, elbow, and wrist pitch torques [Nm] vs. time [s]

have been applied to our controller implementation. Compliance control is paramount when using rigid manipulators to ensure aircraft stability. Insertion-style task results confirm the kinematic and dynamic model and controller for the system. In the future, we plan to compare these results with flight tests performing similar insertion tasks.

REFERENCES

[1] B. Mayton, L. LeGrand, and J. R. Smith, "Robot, feed thyself: Plugging in to unmodified electrical outlets by sensing emitted ac electric fields," in *Robotics and Automation (ICRA), 2010 IEEE International Conference on*. IEEE, 2010, pp. 715–722.

[2] S. Kim, S. Choi, and H. J. Kim, "Aerial manipulation using a quadrotor with a two dof robotic arm," in *IEEE/RSJ International Conference on Intelligent Robots and Systems*, Tokyo, Japan, 2013.

[3] F. Huber, K. Kondak, K. Krieger, D. Sommer, M. Schwarzbach, M. Laiacker, I. Kossyk, S. Parusel, S. Haddadin, and A. Albu-Schaffer, "First analysis and experiments in aerial manipulation using fully actuated redundant robot arm," in *IEEE/RSJ International Conference on Intelligent Robots and Systems*, Tokyo, Japan, 2013.

[4] K. Kondak, K. Krieger, A. Albu-Schaeffer, M. Schwarzbach, M. Laiacker, I. M. A. Rodriguez-Castano, and A. Ollero, "Closed-loop behavior of an autonomous helicopter equipped with a robotic arm for aerial manipulation tasks," in *International Journal of Advanced Robotic Systems*, 2013.

[5] A. E. Jimenez-Cano, "Control of an aerial robot with multi-link arm for assembly tasks." in *IEEE Int. Conf. Robotics and Automation (ICRA)*, 2013.

[6] V. Lippiello and F. Ruggiero, "Exploiting redundancy in cartesian impedance control of uavs equipped with a robotic arm," in *Intelligent Robots and Systems (IROS), 2012 IEEE/RSJ International Conference on*, 2012, pp. 3768–3773.

[7] C. Korpela, M. Orsag, M. Pekala, and P. Oh, "Dynamic stability of a mobile manipulating unmanned aerial vehicle," in *Proc. IEEE Int Robotics and Automation (ICRA) Conf*, 2013.

[8] M. Orsag, C. Korpela, and P. Oh, "Modeling and control of MM-UAV: Mobile manipulating unmanned aerial vehicle," in *Proc.International Conference on Unmanned Aircraft Systems, ICUAS*, 2012, Pending Review.

[9] J. F. Broenink and M. L. J. Tiernego, "Peg-in-hole assembly using impedance control with a 6 dof robot," in *Proceedings 8th European Simulation Symposium*, 1996.

[10] G. M. Hoffmann, H. Huang, S. L. Wasl, and E. C. J. Tomlin, "Quadrotor helicopter flight dynamics and control: Theory and experiment," in *In Proc. of the AIAA Guidance, Navigation, and Control Conference*, 2007.

[11] R. E. Mahony, V. Kumar, and P. Corke, "Multirotor aerial vehicles: Modeling, estimation, and control of quadrotor," *IEEE Robot. Automat. Mag.*, pp. 20–32, 2012.

[12] S. Bouabdallah, P. Murrieri, and R. Siegwart, "Design and control of an indoor micro quadrotor," in *Proc. IEEE Int. Conf. Robotics and Automation ICRA '04*, vol. 5, 2004, pp. 4393–4398.

[13] O. Bourquardez, R. Mahony, N. Guenard, F. Chaumette, T. Hamel, and L. Eck, "Image-based visual servo control of the translation kinematics of a quadrotor aerial vehicle," *Robotics, IEEE Transactions on*, vol. 25, no. 3, pp. 743–749, 2009.

[14] H. Romero, R. Benosman, and R. Lozano, "Stabilization and location of a four rotor helicopter applying vision," in *American Control Conference*, 2006.

[15] L. Tsai and A. Morgan, "Solving the kinematics of the most general six- and five-degree-of-freedom manipulators by continuation methods," in *J. of Mech., Trans, and Automation*, 1985.

[16] N. Hogan, "Impedance control: An approach to manipulation," in *Proc. American Control Conf*, 1984, pp. 304–313.

[17] V. Narli and P. Y. Oh, "Hardware-in-the-loop test rig to capture aerial robot and sensor suite performance metrics," in *Proc. IEEE/RSJ Int Intelligent Robots and Systems Conf*, 2006, pp. 3521–3526.

[18] C. Korpela, M. Orsag, Y. Jun, P. Brahmbhatt, and P. Oh, "A hardware-in-the-loop test rig for aerial manipulation," in *Unmanned Aircraft Systems (ICUAS), 2013 International Conference on*, 2013, pp. 982–987.